International Journal of Applied Earth Observation and Geoinformation 122 (2023) 103432

Contents lists available at ScienceDirect

International Journal of Applied Earth Observation and Geoinformation

journal homepage: www.elsevier.com/locate/jag

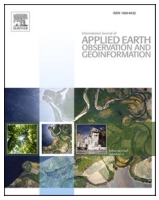

Megalopolitan-scale ground deformation along metro lines in the Guangdong-Hong Kong-Macao Greater Bay Area, China, revealed by MT-InSAR

Bochen Zhang [a,b], Xianing Liao [a,b], Jiayuan Zhang [a,b], Siting Xiong [c], Chisheng Wang [a,d], Songbo Wu [e], Chuanhua Zhu [a,d], Jiasong Zhu [a,b,*], Xiaoqiong Qin [b], Qingquan Li [a,b,c]

[a] MNR Key Laboratory for Geo-Environmental Monitoring of Great Bay Area & Guangdong Key Laboratory of Urban Informatics & Shenzhen Key Laboratory of Spatial Smart Sensing and Services, Shenzhen University, 518060 Shenzhen, China
[b] College of Civil and Transportation Engineering, Shenzhen University, 518060 Shenzhen, China
[c] Guangdong Laboratory of Artificial Intelligence and Digital Economy (SZ), 518000 Shenzhen, China
[d] School of Architecture & Urban Planning, Shenzhen University, 518060 Shenzhen, China
[e] Department of Land Surveying and Geo-Informatics, The Hong Kong Polytechnic University, Kowloon, Hong Kong, China

ARTICLE INFO

Keywords:
Guangdong-Hong Kong-Macao Greater Bay Area (GBA)
Multi-temporal InSAR
Ground deformation
Metro system
Risk assessment

ABSTRACT

As one of the most densely populated and rapidly growing metropolitan areas worldwide, the Guangdong-Hong Kong-Macao Greater Bay Area (GBA) of China has been developing extensive metro networks to relieve the escalating traffic congestion inner cities and to shorten public transport time inter cities. Metro construction possibly triggers ground deformation, which may result in damage to the tunnel, pipeline, and ground structures. Fast and efficient monitoring ground deformation along metro lines is vital not only to the metro itself but also to these structures. This study provides a comprehensive investigation of ground deformation along 67 metro lines within the GBA, based on multi-temporal synthetic aperture radar interferometry (MT-InSAR) by using Sentinel-1 from March 2017 to February 2022. The results reveal that deformation velocity in this area ranges from –39.4 mm/year to 14.2 mm/year, which is mainly caused by the tunnel excavation, adjacent excavation and construction, and unfavorable geological conditions. Furthermore, risk levels have been evaluated based on the InSAR-derived results with the proposed median absolute deviation heatmap clustering method. The risky area accounts for 16.31% (~205.24 km^2) of the whole study area in the GBA, among which 13.76%, 2.16%, and 0.39% are classified as three risk levels, with mean deformation velocities of –2.2 mm/year, –3.4 mm/year, and –6.5 mm/year, respectively. This study presents a comprehensive megalopolitan-scale ground deformation monitoring, for the first time, along metro lines in six cities of the GBA, which provides important insights into future metro line constructing, operating and planning.

1. Introduction

The Guangdong-Hong Kong-Macao Greater Bay Area, commonly known as the Greater Bay Area (GBA), is a burgeoning world-class metropolis in southern China. It includes nine cities of Guangdong province and two special administrative regions, of which six cities (Guangzhou, Hong Kong, Macao, Shenzhen, Foshan and Dongguan) have developed efficient rapid rail transit (also called metro) or light rail systems for their urban populations. Based on statistical data released by the Ministry of Transport of the People's Republic of China, Hong Kong Mass Transit Railway (MTR) Cooperation Limited, and Macao Light Rapid Transit Cooperation Limited, the urban rail transit system in the GBA witnessed a passenger volume of 5.8 billion in 2022, which represented almost 27.8% of the national total (20.9 billion). To enhance transport accessibility, the concept of a "one-hour living circle" has been advocated by local governments. To this end, constructing metro systems and intercity railways has been experiencing accelerating growth in the GBA.

In megacities around the world, such as London, New York, Tokyo, Hong Kong, and Shanghai, developing an urban rail transit system has become a widespread strategy to alleviate the pressure on daily commutes and escalating urban traffic congestion. In 2020, the cumulative

* Corresponding author at: College of Civil and Transportation Engineering, Shenzhen University, 518060 Shenzhen, China.
E-mail address: zhujiasong@gmail.com (J. Zhu).

https://doi.org/10.1016/j.jag.2023.103432
Received 16 April 2023; Received in revised form 11 July 2023; Accepted 23 July 2023
Available online 2 August 2023

length of constructed metro lines in the GBA exceeded 1,000 km; moreover, an incredible additional 886.4 km is planned to be completed by the end of 2025 (according to the Guangdong Province integrated transportation system "14th Five-Year" development plan published in 2021). With expanding rail transit systems, accidents world widely occur during the construction and operation periods, owing to causal factors like the unsafe operation of constructors, technical failures, environmental and geological issues, and improper management (Kyriakidis et al., 2012; Sousa and Einstein, 2021; Zhou et al., 2021). For metro systems, one of the most catastrophic accidents is ground collapse, often associated with substantial deformation of metro line segments and resulting in significant damages to both the metro tunnel and ground structure. For example, during the construction in 2008, the Hangzhou subway (Line 1) suddenly collapsed due to a series of 11 sub-accidents, leading to an unfortunate loss of 21 lives and caused injuries to 24 individuals (Zhou and Irizarry, 2016). Similar catastrophic events also occurred in other regions and countries, notably, the Lausanne Metro Line M2 collapse in 2005, the Foshan Metro Line 2 collapse in 2018, the Mexico City Metro overpass collapse in 2021, and the San Paulo Subway Line 6 collapse in 2022 (Zhu et al., 2022). Ground deformation during both the construction and operational phases may have a notable impact on the metro system as well as surrounding structures and utilities, potentially leading to catastrophic events. Monitoring the ground deformation along metro lines, therefore, is vital to enable early identification of risks and evaluate the potential impact of surrounding structures on the metro line and the effect of metro construction on the surrounding structures.

Directly monitoring the deformation of metro lines can be challenging due to a variety of reasons, such as the concealed and narrow space, complex environment during construction, fully enclosed operation, and extensive linear distribution. Techniques commonly employed for deformation monitoring along metro lines, from the ground or inside the tunnel, can be typically categorized as contact sensors (i.e., electronic liquid level gauges and optical fiber), geodetic techniques(i.e., total station, terrestrial laser scanning and global positioning system), and geotechnical methods (i.e., tiltmeters and inclinometers) (Kavvadas, 2005; Zhou et al., 2020). However, these techniques are either of low sampling rate or high expense for extensive metro lines, thereby their capacity to provide comprehensive deformation information for the entire metro line at the city or metropolitan scale is limited.

Satellite synthetic aperture radar interferometry (InSAR) has demonstrated its capability to provide remote sensing of ground deformation across a wide range, such as the whole GBA area (Ma et al., 2019). It enables deformation monitoring to be conducted during day and night, regardless of weather conditions and offers a remarkable precision ranging from centimeters to millimeters (Ferretti et al., 2011). In comparison to conventional surveying methods, InSAR offers the distinct advantage of providing a higher density of measurement points over large areas, including hazardous or difficult-to-access regions (Marghany, 2012, 2014a, b). Owing to these capabilities, the investigation of the spatiotemporal deformation along metro lines has been studied extensively using the multitemporal InSAR (MT-InSAR) (Giardina et al., 2019; Perissin et al., 2012), particularly for city-scale metro network (Duan et al., 2020; Hu and Li, 2021; Liao et al., 2022; Wang et al., 2017; Wang et al., 2022) that have experienced significant fissure and collapse (Gheorghe et al., 2020; Wu et al., 2021; Yang et al., 2022; Zhu et al., 2020). In addition, a method based on thresholding deformation velocities, relative velocities, and cumulative displacement is adopted for evaluating the level condition of PS points along Shanghai metro lines (Yang et al., 2022). This study presents a comprehensive analysis of metropolitan-scale ground deformation along the entire metro lines in GBA utilizing multitemporal Sentinel-1 data from March 2017 to February 2022. The study aims to investigate the spatiotemporal ground deformation along metro lines at different stages of their life period and provide insights into the risky deformation occurring within the entire metro system of the GBA.

2. Overview of GBA urban transit systems

2.1. Study area and geological condition

The GBA megalopolis, located in the coastal area of South China around the Pearl River estuary, as shown in Fig. 1, has emerged as one of the largest and fastestgrowing urban regions in the world. Covering an expansive area of approximately 56,000 km^2, it is home to over 86.7 million residents and contributes the gross domestic product (GDP) of over $1.95 trillion by the end of 2021. The GBA primarily consists of deltaic plains, which have been formed through millennial cycles of alluvial sedimentation resulting from the interplay of land and sea. In addition, the region exhibits several scattered topographical features,

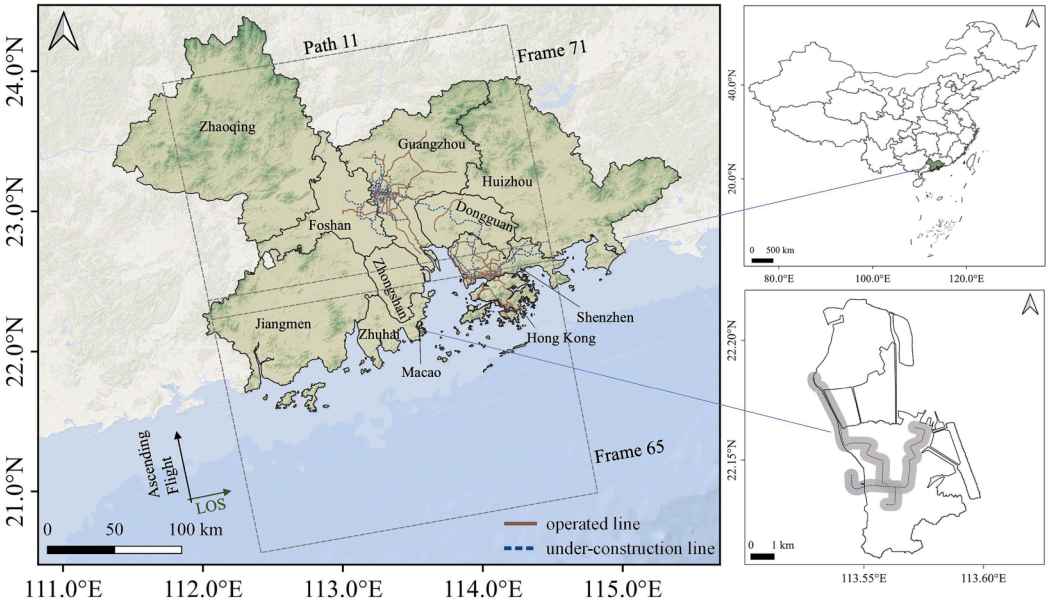

Fig. 1. Geological distribution of the GBA area.

such as hills, plateaus, and monadnocks. The Quaternary sediments exhibit varying elevations in GBA, with the northern region ranging from 6 to 9 m above sea level, while the coastal area is 1–2 m (Wang and Jiao, 2012). The rapid economic expansion has led to a proliferation of anthropogenic activities in GBA, resulting in multiple geological hazards, such as ground subsidence (around reclaimed land, constructed land, and silty soft or sandy soil), fissures (ground and buildings), sink hole, unstable slope, landslide, flood, and urban waterlogging (Lancia et al., 2020; Ma et al., 2019). According to the statistical data released by the Department of Natural Resources of Guangdong Province, by the end of 2020, a total of 1,468 danger locations related to geological hazards had been reported within the GBA (except Hong Kong and Macao), thereby posing a significant threat to over 4,500 individuals and leading economic losses more than 1.8 billion yuan.

2.2. Construction environment of the urban transit systems

The urban transit system, which typically encompasses rapid transit (also called metro) and light rail, is widely recognized as one of the most efficient forms of transportation, which reduces heavy traffic in urban areas. In GBA, the construction of transit systems is expanding rapidly, six out of eleven cities within the GBA have constructed their urban transit systems, including Guangzhou, Hong Kong, Macao, Shenzhen, Foshan and Dongguan. At the beginning of 2022, a total of 42 operational metro and light metro lines covering a length exceeding 1,378 km were implemented in these cities, with an additional 25 planned lines under construction, as summarized in Table 1. Among these cities, the mass transit railway system in Hong Kong is comparatively well-developed, with a network of 12 operational metro and light metro lines. Guangzhou and Shenzhen possess relatively extensive metro systems, both with a length exceeding 400 km and several lines in planning. On the other hand, the development of metro lines in Macao, Foshan and Dongguan is limited as there are smaller populations.

The overall geological conditions in the GBA are highly complex and heterogeneous, which raises challenges to the metro system construction. In Guangzhou, the presence of karst strata, Quaternary loose sediments, active faults, and high piezometric level of fissure water makes the constructed terrain susceptible to three types of potential geohazards, namely water ingress and strata erosion, ground subsidence, and sinkhole (Ren et al., 2016). In Shenzhen, the western region is characterized by thin (0 to 40 m) and uneven Quaternary sediments, whereas the eastern region, particularly in the Longgang district, is dominated by a large area of karst strata. Moreover, the development of problematic soil, including granite residual soil, muddy clay and silt, further adds to the geological diversity of Shenzhen (He et al., 2020). In Hong Kong, the terrain is characterized by rugged terrains, primarily underlain by granitic, volcanic rocks, and the natural deposit in the region mainly consists of alluvial flats, residual soil, and colluvium (Linney, 1983). In addition, intensive land reclamations have been undertaken along the coastal margins of the GBA, particularly in Hong Kong, Macao, Guangzhou, and Shenzhen. In these cities, a significant portion of metro lines was built on the newly reclaimed regions, which had undergone a lengthy consolidation process.

3. Data and method

3.1. Data

To obtain the ground deformation across a large study area, 292 (146 epochs) ascending Sentinel-1A SAR data spanning from March 12, 2017, to February 2, 2022, were collected from two adjacent frames (65 and 71). These data are used to monitor the deformation along metro lines within the GBA, as illustrated in Fig. 1. A digital elevation model (DEM) from the ALOS Global Digital Surface Model (DSM), named AW3D30, with a spatial resolution of 30 m, is adopted to remove topographic phase and geocoding estimated deformation. Shapefiles of the constructed and under-constructed metro lines from the OpenStreetMap and OpenRailwayMap are used to generate buffer zones (300 m) around the study area. Global positing system (GPS) measurements at two continuous stations (HKFN and DSMG) from the Nevada Geodetic Laboratory (Blewitt et al., 2018) were used to validate the InSAR results in the overlap regions.

3.2. InSAR data processing

The interferometric processing in this study was implemented by using GAMMA software (Werner et al., 2000), including concatenation of consecutive burst single look complex (SLC) images, coregistration, mosaics of sub-swaths SLCs, the removal of flat-earth and topographic phases, interferogram formation, and geocoding. Precise orbit ephemerides for Sentinel-1 are used to refine the orbit state vectors of each SLCs.

After the interferometric processing, we generate a 300 m butter zone surrounding each of the metro lines city-by-city, and retrieve line-of-sight (LOS) deformation within the buffer zone by using the Stanford method for persistent scatterers (StaMPS) based persistent scatterers InSAR (PS-InSAR) (Hooper et al., 2004). The amplitude dispersion and phase stability analysis were combined to detect the persistent scatterers (PS), and in this study, the thresholds of these two indicators were set as 0.4 and 0.6, respectively. Three-dimensional (3D) Phase unwrapping is implemented after eliminating spatially correlated look angle error and master atmosphere and orbit error. Mean values for the whole area are used as the reference for phase unwrapping, which is almost close to zeros. The atmospheric phase effect at each coherent point was mitigated by using high-pass and low-pass filtering in time and space, respectively.

In urban environments, thermal expansion can introduce significant biases to InSAR deformation time series (Wu et al., 2020), particularly in relation to infrastructures such as buildings, railway stations, and roads. We use the daily air temperature on the SLC acquisition date to correct the thermal expansion phase for all points in each city. The correction model can be expressed as $d_{\Delta T} = k\Delta T + c$, where k is the thermal

Table 1
Overview of metro systems in GBA.[a]

City	Operational lines	Length in operation [km]	Constructed lines or segments	Length under construction [km]	Opened year
Hong Kong	11	274.55	1	10.98[b]	1980
Guangzhou	15	581.23	10	304.31	1997
Shenzhen	12	421.34	9	220.50	2004
Foshan	2	53.88	1	40.72	2010
Dongguan	1	37.74	1	57.50	2016
Macao	1	9.30	3	6.90	2019
Total	42	1367.06	25	640.91	

[a] Data were collected from https://baike.baidu.com/item/%E5%9C%B0%E9%93%81/21266? [in Chinese, accessed on February 02, 2022].
[b] The Sha Tin to Central Link is forming into the new Tune Ma line.

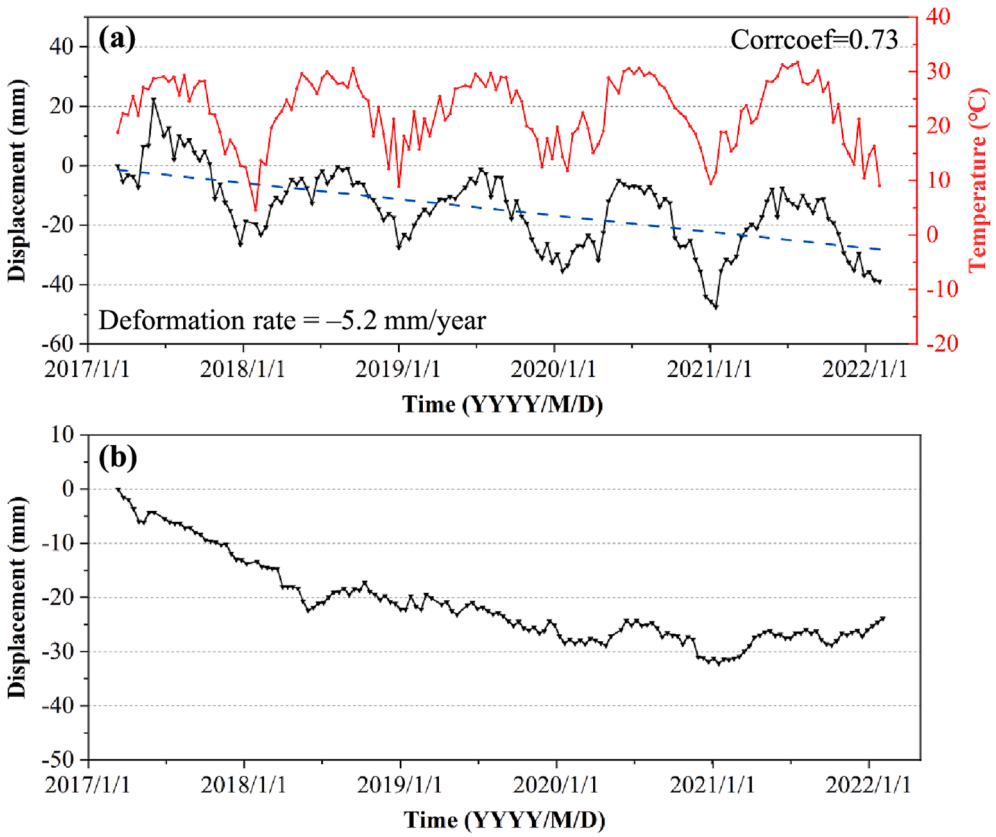

Fig. 2. Thermal expansion correction at a point near the metro station of Huacheng Dadao in Guangzhou. (a) The correlation between the temperature changes and time-series InSAR results. (b) Time-series InSAR results after thermal expansion correction.

expansion factor, ΔT is the temperature changes between two acquisitions, and c is the offset factor. Fig. 2 shows an example of the correction at a point near the metro station of Huacheng Dadao in Guangzhou. The correlation between temperature changes and time-series displacements is 0.73, and the corrected result can more exactly reflect the actual ground deformation.

3.3. Risk assessment

In this section, a risk assessment is carried out based on the InSAR displacement velocities as denoted as a vector, $\boldsymbol{x} = [x_1, x_2, \cdots, x_N]$, of N extracted points, with which the median absolute deviation (MAD) can be calculated as Eq. (1) (Leys et al., 2013).

$$MAD = bM_j\left(\left|\boldsymbol{x}_j - M_i(\boldsymbol{x}_i)\right|\right) \tag{1}$$

where $M(\bullet)$ denotes the median operator, and b is a constant value of 1.4826. For each point in the $\boldsymbol{x}$, a risk index γ can be derived by using the MAD as shown in Eq. (2), and with this index, each point is labelled as $\mathscr{L}$ using Eq. (3) (Miller, 1991).

$$\gamma = \left|\frac{\boldsymbol{x}_i - M_i(\boldsymbol{x}_i)}{MAD}\right| \tag{2}$$

$$\mathscr{L} = \begin{cases} 0 & \gamma \le 2 \\ 1 & 2 < \gamma \le 2.5 \\ 2 & 2.5 < \gamma \le 3 \\ 3 & 3 \le \gamma \end{cases} \tag{3}$$

For each type of point in Eq. (3), we produce a heatmap with a quartic kernel shape and a radius of 600 m to reflect the density of risky points. For justifying the inhomogeneity of the InSAR selected points, the heatmap is weighted by using the division between the risk index and the number of points within a radius (set as 1 km in this case), $w = \mathscr{L}/\mathrm{n}$. Therefore, the heatmap not only reflects the density but also reflects the significance of risky points. The heatmap values have no physical meaning and are standardized to be 0 to 1. It is zeros when $\mathscr{L} = 0$, therefore, only the other three heatmaps are summarized. Following, to determine a risk level along the metro lines, the K-means clustering method (Hartigan and Wong, 1979) is used to further cluster the pixel value of the heatmap into four clusters, including one class of normal points (L0) and three classes of increasing risk (L1–L3).

4. Results

4.1. Overall Megalopolitan-scale deformation

Based on the single master processing chain, 145 interferometric image pairs are generated, as the spatiotemporal network shown in Fig. 3. We then obtained the ground deformation along metro lines within the GBA city-by-city using the method in section 3.2. Almost five years of ground deformation between March 12, 2017, to February 2, 2022, within the 300 m buffer zone of 67 metro lines, are extracted as shown in Fig. 4. Overall, the results suggest that the derived LOS deformation velocity is spanning from –39.4 mm/year to 14.2 mm/year, of which 99.89% varies from –12.0 mm/year to 12.0 mm/year. As illustrated in Fig. 4, the coherent points exhibit a high density along metro lines, but they are sparsely distributed in areas with dense vegetation (e.g., Line 21 around the Huangpu Youma Shan Forest Park in Guangzhou and Tuen Ma Line around the Lin Fa Shan in Hong Kong) and areas undergoing extensive construction activity (e.g., Line 11 around the north of the Shenzhen Bao'an International Airport, SBIA and Line 21 in close to the Shenzhen World Exhibition & Convention Center).

The results also suggest that the ground buffer zone along metro lines is relatively stable in most areas of GBA, with LOS deformation velocity between –5.0 mm/year and 5.0 mm/year. Significant regional

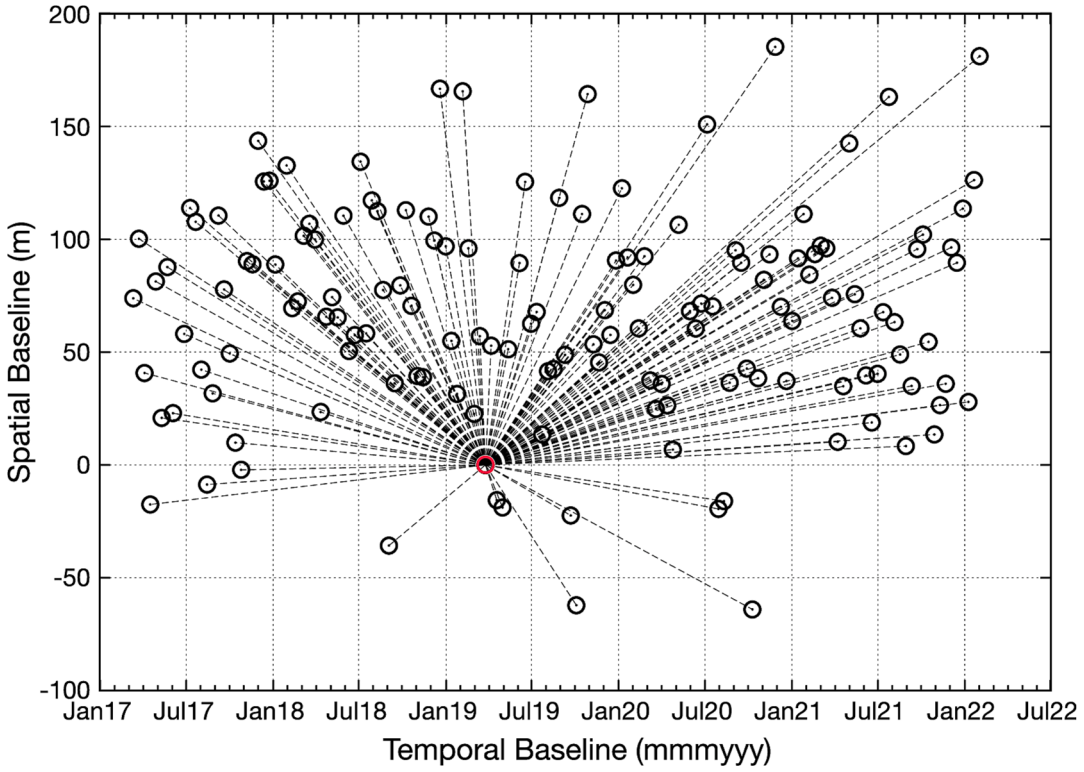

Fig. 3. Spatial-temporal baselines configuration of the generated interferograms. The red circle represents the referenced image (20190326).

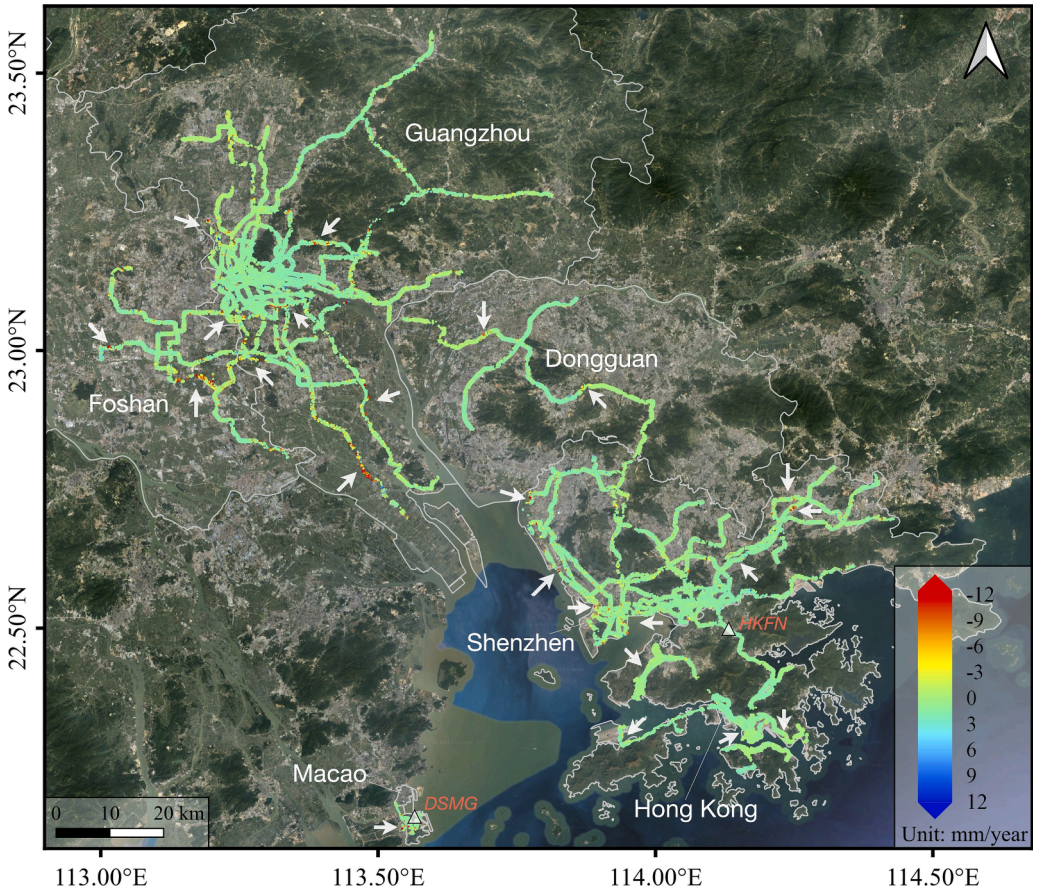

Fig. 4. InSAR LOS ground deformation velocity map along the metro lines (within a buffer zone of 300 m), between March 12, 2017, to February 2, 2022, derived from Sentinel-1A data. The white triangles denote the location of the two GPS stations (HKFN and DSMG). The white arrows indicate the regions with significant deformation.

Fig. 5. Severe deformation near metro lines within the GBA, (a)–(b) structures displacement near the Shangchuan Station in Shenzhen, as seen in Fig. 7 (f), (c) building subsidence near the Foshan Poly Plaza (from Baidu Street View), (d) collapse of the "2018 Foshan 2.7 event" along Line 2 (see Fig. 8 (b)), (e) collapse of the "2019 Guangzhou 12.1 event" along Line 11, (f) road fissure and wall crack near the Shenzhen Bay Sports Center, (g) wall crack near the To Kwa Wan Station in Hong Kong.

deformation happened primarily in the southeastern region of the Nansha district in Guangzhou, as well as in certain areas within the Nanshan and Bao'an districts of Shenzhen, and areas north of the Shunde district in Foshan, as the regions annotated by the white arrows in Fig. 4. Ground deformation may result from different diverse factors, such as geology conditions and anthropogenic activities. The photos of field investigation related to severe deformation in surrounding structures are shown in Fig. 5. These causing factors of the deformation along metro lines are different in different cities, and they are detailly analyzed in section 4.2.

4.2. City-scale deformation in the GBA

(1) Hong Kong mass transit railway (MTR)

Hong Kong MTR was the earliest constructed metro system in the GBA, whose construction started in 1980. It now consists of 11 metro and light metro lines (see Table 1), which are open to public service. All the metro lines had been operated for many years before the monitoring period started, during which only the Sha Tin to Central Link was under construction and it commenced in May 2022. All the metro lines in Hong Kong have been constructed beneath or on segments of the reclaimed lands after a long term of ground settlement and consolidation. The derived InSAR deformation velocity along metro lines in Hong Kong ranges from –16.4 mm/year to 10.7 mm/year in the monitoring period, and the deformation velocity map is demonstrated in Fig. 6. Therefore, deformation along the metro lines in Hong Kong is not related to metro construction itself; instead, it is more associated with the updating of other urban infrastructure or other anthropogenic activities.

(2) Guangzhou metro

The metro system in Guangzhou is the densest and longest among cities in the GBA, with a total number of 25 metro lines, and 10 of them are under construction during the monitoring period. Two ground surface collapsing events that occurred on January 25, 2018 (Line 21) and December 01, 2019 (Line 11), respectively, were caused by the construction of the metro line (Zhu et al., 2022). From the InSAR-derived deformation velocity map shown in Fig. 7, remarkable deformation can be observed along the under-constructed metro lines (e.g., segments of Lines 8, 11, 13, and 22) and in the southeastern region of the Nansha district, with the deformation velocity of –39.4 mm/year to 14.2 mm/year. The causing factors of the deformation in these areas are inferred primarily to be the construction of the new metro lines and unfavorable geological conditions.

(3) Shenzhen metro

Similar to Guangzhou, extensive construction of metro lines has been conducted in Shenzhen, where nine metro lines are under construction during our monitoring period, mainly in the Nanshan, Bao'an, and Longgang districts. Metro lines in the Nanshan peninsula are partly located within the reclaimed lands. The InSAR-derived deformation velocity along metro lines in Shenzhen ranges from –35.5 mm/year to

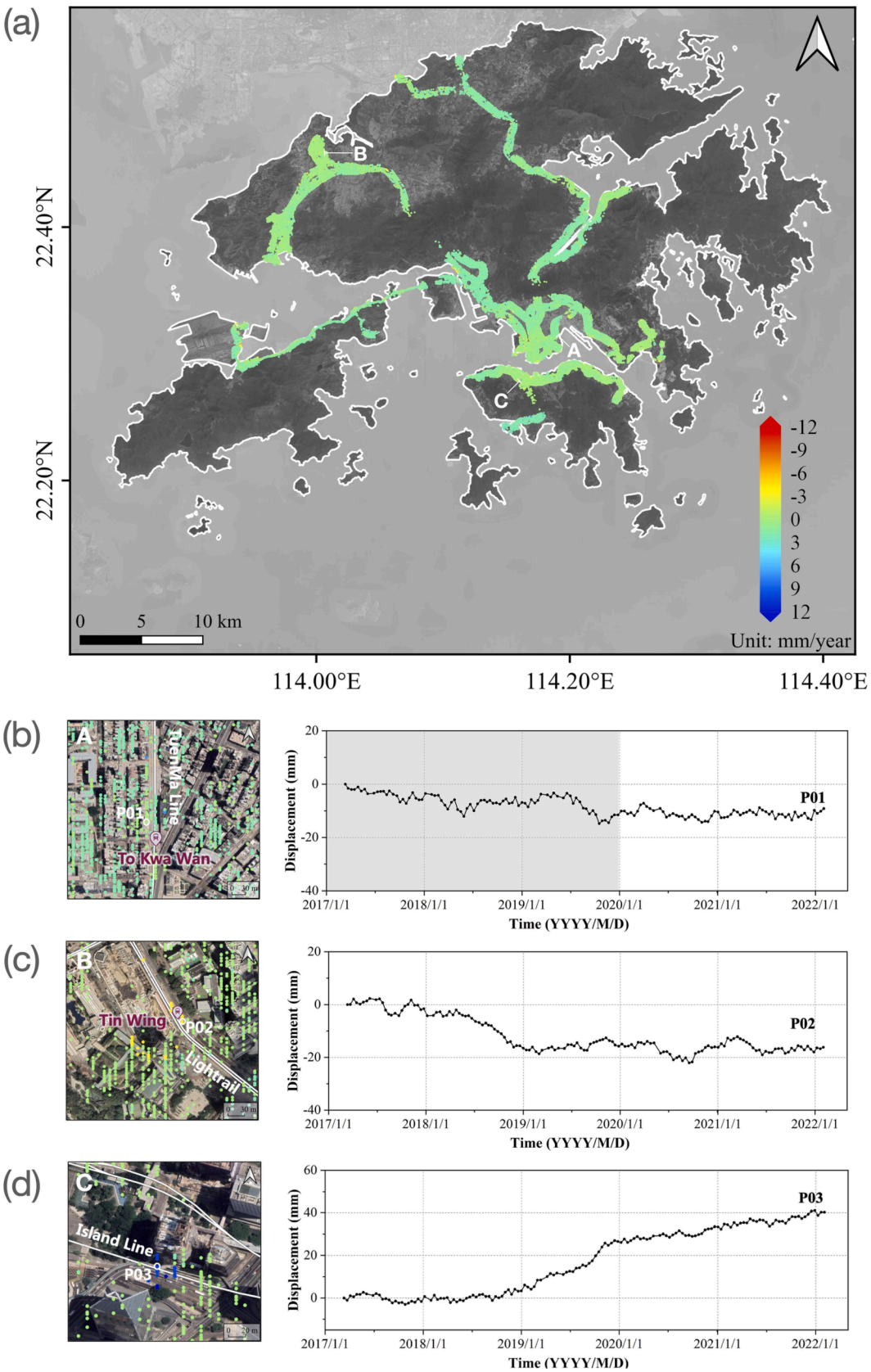

Fig. 6. InSAR-derived deformation maps in Hong Kong. (a) Deformation velocity map, (b)–(d) local deformation velocity in areas A–C, respectively, left panel: displacement velocity, right panel: time series displacement, and the metro construction period is outlined in gray.

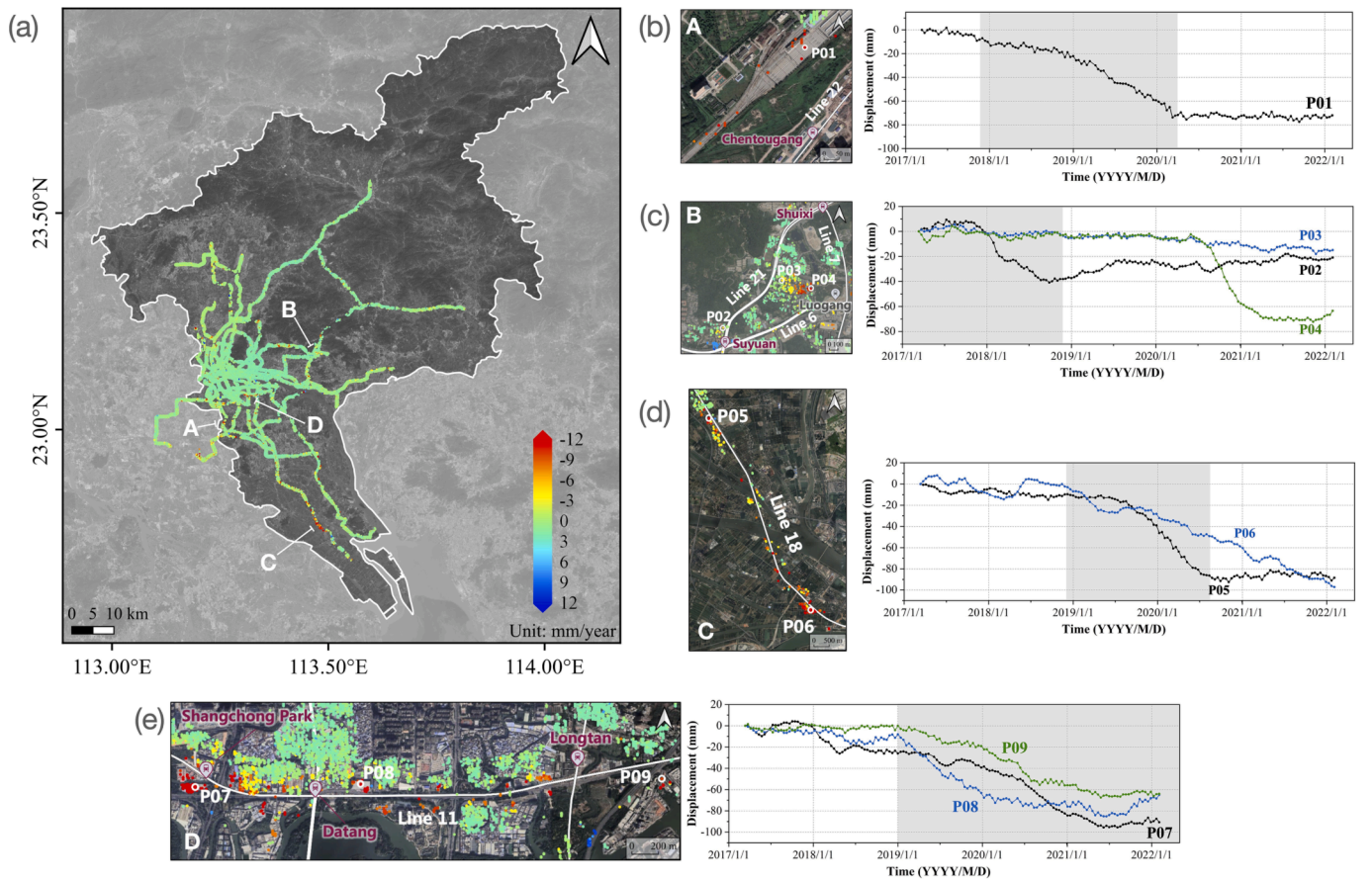

Fig. 7. InSAR-derived deformation maps in Guangzhou. (a) Deformation velocity map, (b)–(c) local deformation velocity in areas A–B, respectively, left panel: displacement velocity, right panel: time series displacement, and the metro construction period is outlined in gray.

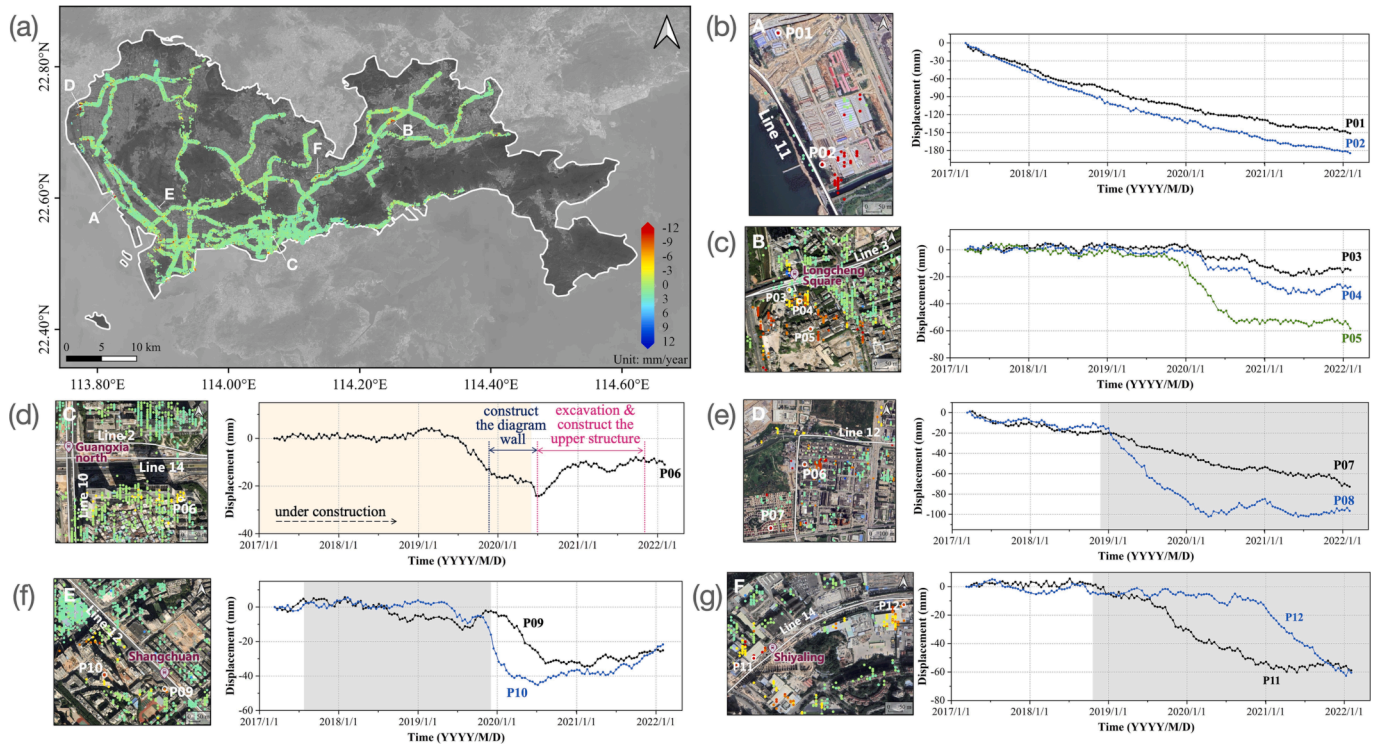

Fig. 8. InSAR-derived deformation maps in Shenzhen. (a) Deformation velocity map, (b)–(g) local deformation velocity in areas A–F, respectively, left panel: displacement velocity, right panel: time series displacement, and the metro and station construction are outlined in gray and beige, respectively.

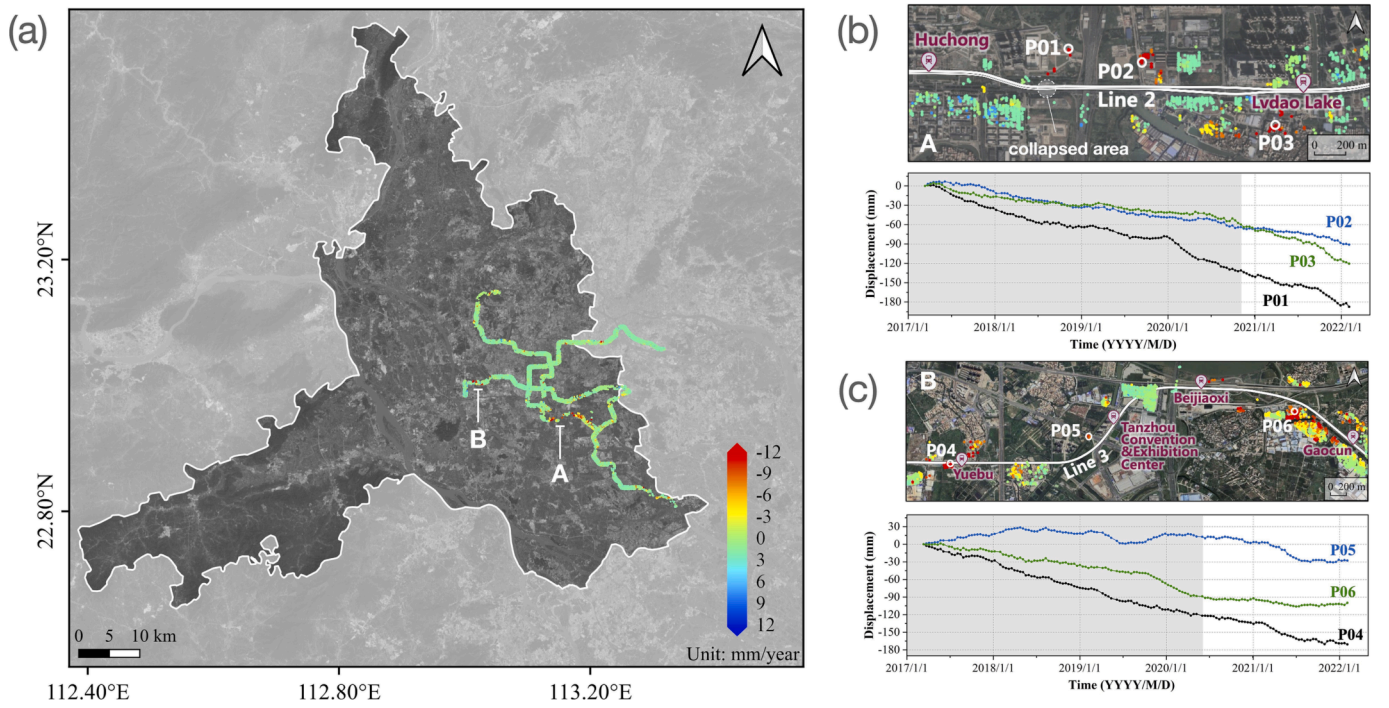

Fig. 9. InSAR-derived deformation maps in Foshan. (a) Deformation velocity map, (b)–(d) local deformation velocity in areas A–C, respectively, left panel: displacement velocity, right panel: time series displacement, and the metro construction is outlined in gray.

12.3 mm/year, as shown in Fig. 8. The InSAR-derived results reveal that the deformation hotspots are sparsely distributed along all the metro lines, which might be related to the rapid development of both ground and underground infrastructure in Shenzhen in the recent years, such as areas within the Nanshan peninsula, around the north and south of SBIA, and Lines 3 and 14 in central of the Longgang district.

(4) Foshan metro

The metro system of Foshan is connected with the metro system of Guangzhou via Guangfo Line and Guangzhou Line 7, and more lines are planned for further connection with Guangzhou. The derived deformation velocity along metro lines in Foshan varies from –34.9 mm/year to 10.9 mm/year. As shown in Fig. 9, significant deformation is detected in the middle segment of Line 3 and the collapsed region of the "2018–02-07 Foshan collapse event", which will be discussed in section 5.1.

(5) Dongguan rail transit

During the monitoring period, there are only two metro lines, namely, Line 2 whose operation started in 2016, and Line 1 which is still under construction. Compared with other cities, the ground surface along metro lines in Dongguan is relatively stable. The obtained ground deformation velocity by using InSAR ranges from –22.2 mm/year to 9.3 mm/year. Line 1 suffers from larger deformations as seen from the area annotated by the white line in Fig. 10.

(6) Macao light rapid transit

The metro system in Macao consists of one light rail line already constructed and three lines under construction, all of which are built above the ground with viaduct structures and stations, except the Hengqin extension Line which is currently built in an underwater

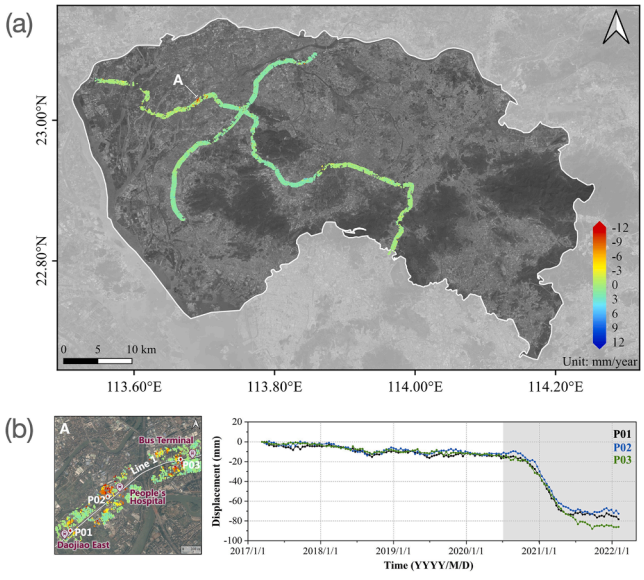

Fig. 10. InSAR-derived deformation maps in Dongguan. (a) Deformation velocity map, (b) local deformation velocity in areas A, left panel: displacement velocity, right panel: time series displacement, and the metro construction is outlined in gray.

tunnel. The InSAR-derived ground deformation along the light rail lines in Macao ranges from –37.0 mm/year to 9.7 mm/year. As seen from areas annotated by the white line in Fig. 11, the large ground deformation occurs in areas under construction or surrounding buildings.

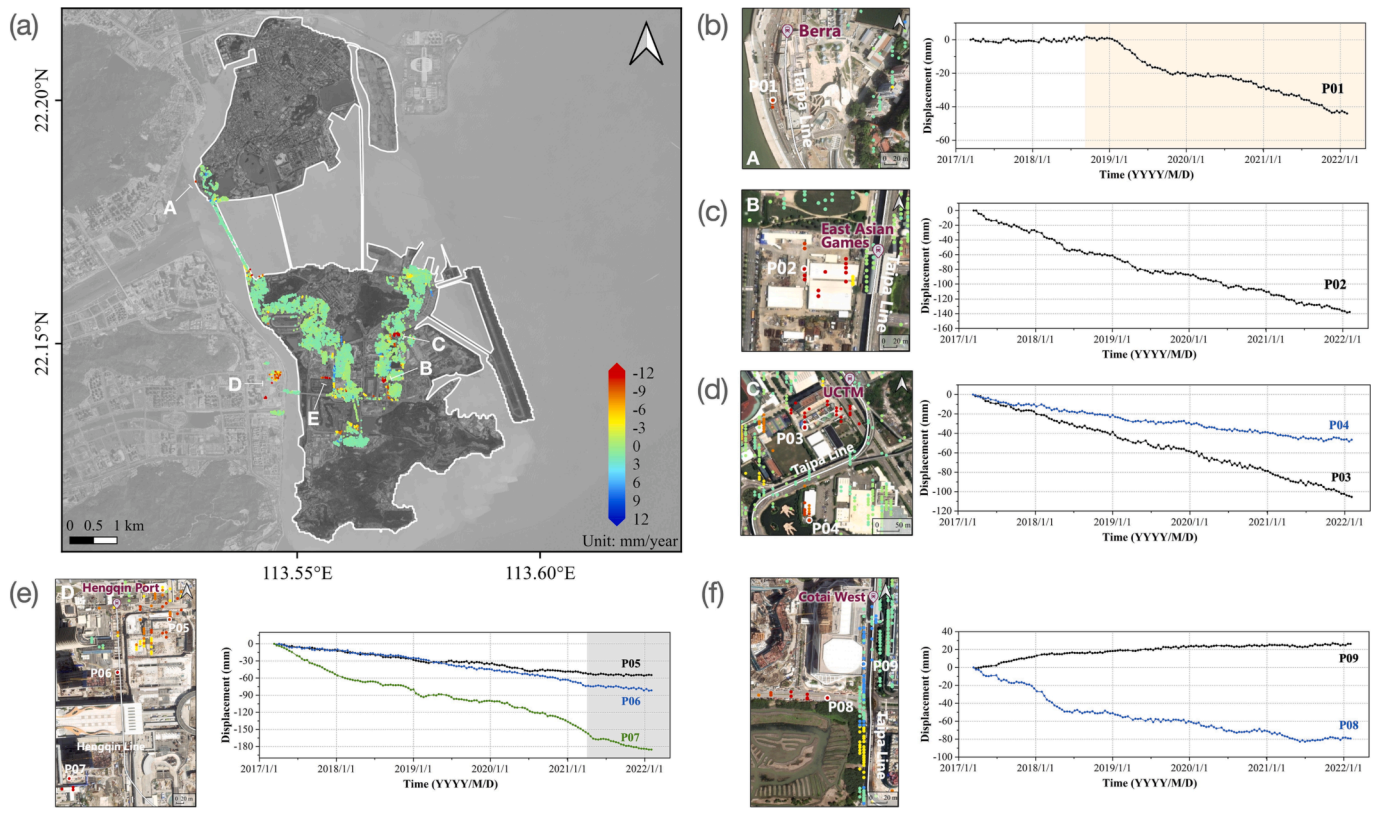

Fig. 11. InSAR-derived deformation maps in Macao. (a) Deformation velocity map, (b)–(f) local deformation velocity in areas A–E, respectively, left panel: displacement velocity, right panel: time series displacement, and the metro and station construction are outlined in gray and beige, respectively.

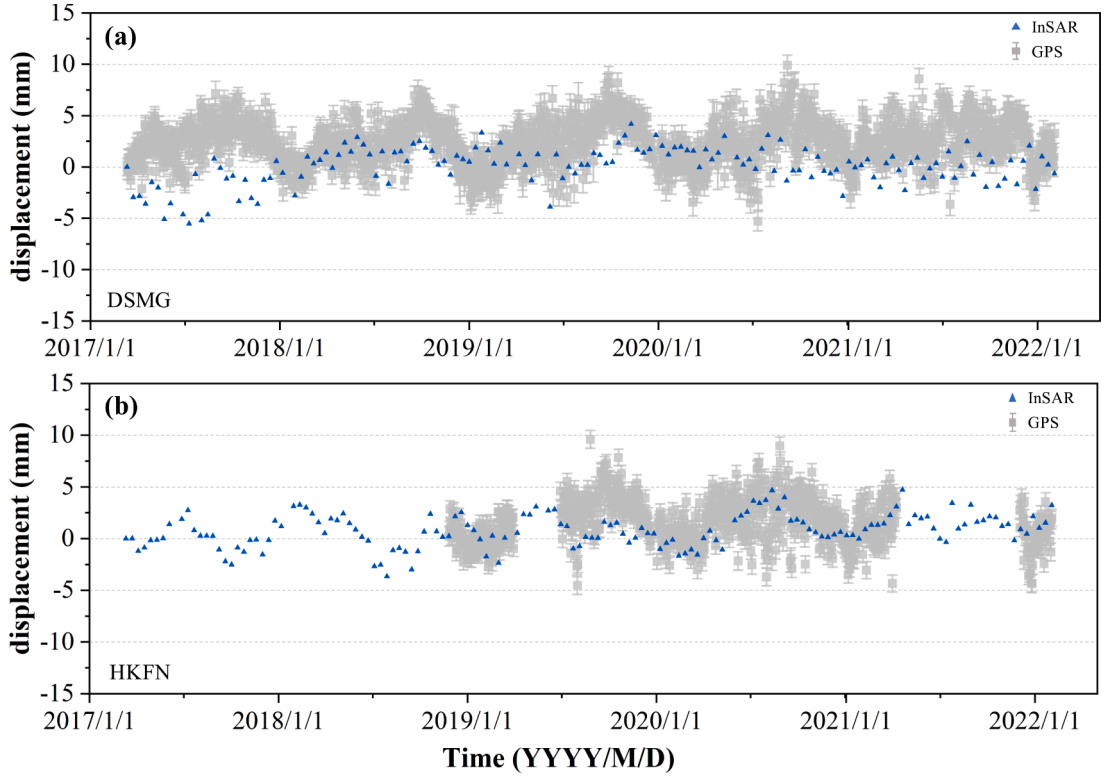

Fig. 12. Time series deformation results from GPS and InSAR at stations of (a) DSMG and (b) HKFN, respectively. Gray boxes represent the GPS data, and blue triangles denote the InSAR results. For each epoch, the InSAR results at one point are averaged from its surrounding 20 points. (For interpretation of the references to colour in this figure legend, the reader is referred to the web version of this article.)

4.3. Validation

To validate the InSAR-derived LOS deformation, we use the GPS network distributed in Hong Kong and Macao, which has a total number of 29 continuous GPS stations, and the GPS data is released by the Nevada Geodetic Laboratory. However, only three stations, HKFN, DSMG, and HKO1, are within or near the buffer zone, and data of HKO1 starts from October 2019, which accounts for a temporal overlap of only five-month with the monitoring period. We, therefore, use the GPS observations at HKFN and DSMG to validate the derived InSAR time-series deformation. Median interannual difference adjusted skewness (MIDAS) is adopted to detrend the original GPS time series results in north, east, and up directions simultaneously, which is resistant to seasonal signals, outliers, discontinuities, and heteroscedasticity in time series GPS data (Blewitt et al., 2016). After detrending, we convert the three directions of GPS deformation to LOS direction. The results from GPS are consistent with the derived InSAR deformation at the HKFN and DSMG stations, as seen from the comparison demonstrated in Fig. 12. And the root-mean-square error (RMSE) between GPS and InSAR deformation measurements is 3.3 mm.

5. Discussion

5.1. Causes of the ground deformation along metro lines

Deformation occurring along metro lines can result from a range of interconnected or accompanied factors, including extensive excavation, internal and external loads, fissure water, pipeline rupture, heavy rainfall, broken rock mass, geological conditions, reinforcement or consolidation, and land reclamation. Deformation caused by these factors can potentially result in damage to the tunnel, underground pipeline, and nearby aboveground infrastructures. In Table 2, linear trend and cumulative deformation along metro lines for all six cities are summarized with regard to their typical causing factors.

(1) Tunnel excavation

During our observation period, 25 metro lines in the GBA are being constructed, mainly in Guangzhou and Shenzhen. Deformation related to the tunnel construction is often triggered by accompanied causes, such as improper construction, unfavorable geological conditions (i.e., faults, karst strata, and water-rich strata), rock stress imbalance, and extremely hydrological conditions (i.e., water ingress and groundwater change) (Ren et al., 2016; Zhu et al., 2022). During the excavation, ground deformation and even collapse are often associated with the progress of tunneling due to the aforementioned reasons. As shown in Fig. 6–Fig. 11, the time series displacement highlighted in gray indicates the under-construction period of metro lines, and the results demonstrate that deformation is highly correlated with construction activities. Taking the area-A of Dongguan Line 1 as an example (see Fig. 10 b), from Daojiao East Station to Bus Terminal Station, the area was slowly deformed from the begging to the middle of 2020 on P01–P03, followed by a rapid subsiding trend that was observed from September 2020 with a maximum cumulated displacement of –86.0 mm on P03. This type of deformation is obvious in regions of other cities with metro construction within GBA, such as P01–02 and P05–09 in Guangzhou, P07–08 and P11–12 in Shenzhen, and P01–06 in Foshan. In addition, the result shows that large excavation-induced deformation no longer continues to develop after the excavation is finished in some areas, such as P01 in Hong Kong (To Kwa Wan Station, see Fig. 6b), and P01 in Guangzhou.

Collapse is the most common type of accident resulting from tunnel excavation, which on occasion leads to catastrophic events during the construction of metro lines. Statistical evidence indicates that collapses accounted for 65% of major tunnel construction accidents from 2010 to 2020 in China, causing a total of 172 fatalities and accounting for 59% of all fatalities (Zhu et al., 2022). Three catastrophic collapses occurred in the GBA during the monitoring period, including the “2018–01-25 Guangzhou collapse event” along Line 21, the “2018–02-07 Foshan collapse event” along Line 2, and the “2019–12-01 Guangzhou collapse event” along Line 11. Fig. 9 (b) shows the deformation zone along Line 2 between Huchong Station to Lvdao Lake Station near the location of the “Foshan collapse event”, which is associated with groundwater leakage and soft soil consolidation (Zhu et al., 2020). The results demonstrate that the area on both sides of the segment has experienced substantial deformation since the time of our monitoring, notably, P01, located approximately to the collapsed area, has experienced the largest subsidence with a cumulative displacement of –187.3 mm (see Fig. 9 b).

(2) Adjacent excavation or construction

The foundation pits and buildings constructed adjacent to existing metro tunnels are the secondary factors contributing to ground deformation along metro lines, which unavoidably disrupt the balance of ground stress and rise soil movements in the vicinity of the tunnels (Liang et al., 2018). These activities consequently induce uplift and subsidence, which harm both the underlying tunnels and surrounding infrastructures, potentially resulting in damage to adjacent existing tunnels (Chang et al., 2001).

This type of deformation is prominently evident in Shenzhen, where rapid urbanization is currently taking place. As shown in Fig. 8 (b), the selected coherent point (P06) near the Gangxia North hub experienced a moderate subsidence starting from March to June 2019, which was immediately followed by an uplift trend from June 2019 to September 2021. During the construction of the diagram wall, a subsidence of –11.26 mm occurred, possibly as a result of dewatering. Similar phenomena weredocumented during the construction of diagram walls in Hong Kong (Linney, 1983). Obvious uplift, up to 15.8 mm, is then followed, and probably resulting from a combination of progresses, including the excavation of the whole foundation pit, back pressure and precipitation, and excavation of adjacent sections. This phenomenon is in accordance with the evolution of tunnel uplift recorded in section K4044 (Zhao et al., 2023). The excavation-induced uplift can also be found at P02 in Hong Kong and P09 in Macao.

In addition, adjacent excavation with groundmass loss and partial stress relief can result in ground subsidence, which is an unavoidable risk to underlying tunnels and surrounding buildings. The magnitude and distribution of excavation-induced subsidence depend on the extensiveness of the construction and local geological conditions. Examples of this type of deformation are shown as P02 in Hong Kong (see Fig. 6 (c), constructions nearby Tin Wang Station), P04 in Guangzhou (see Fig. 7 (c), nearby construction of interchange station), P01–P02 (see

Table 2
Detailed deformation information along metro lines within GBA.

City	PS No.	Deformation velocity [mm/year]	Maximum cumulated deformation [mm]	Main causing factors of deformation
Hong Kong	282,087	–16.4 ~ 10.7	–77.0	Source-1[a], Source-2[b]
Guangzhou	606,249	–39.4 ~ 14.2	–171.3	Source-1, Source-2, Source-3[c]
Shenzhen	481,965	–35.5 ~ 12.3	–184.6	Source-1, Source-2, Source-3
Foshan	104,667	–34.9 ~ 10.9	–187.3	Source-1
Dongguan	99,841	–22.2 ~ 9.3	–99.8	Source-1
Macao	12,652	–37.0 ~ 9.7	–185.3	Source-2, Source-3

[a] Source-1: Tunnel excavation.
[b] Source-2: Adjacent excavation or construction.
[c] Source-3: Geological condition.

Fig. 8 (b), nearby construction of the entrance of Shenzhen-Zhongshan Bridge) and P03–P05 (see Fig. 8 (c), nearby construction of buildings) of Shenzhen, and P01–P08 of Macao (see Fig. 11 (b)–(f), nearby construction of structures).

(3) Geological condition

The geological features present varying heterogeneity and complexity across cities within the GBA, as described in section 2. The deformation induced by the geological condition and excavation is often accomplished, such as tunneling under karst terrain that is particularly widely distributed in Guangzhou and northeast of Shenzhen (He et al., 2020; Ren et al., 2016). Deformation and even collapse, sometimes inevitably happened when excavation or construction in areas with the unfavorable geological conditions, as the cases are shown in section 5.1.1. For this reason, we will not discuss it furthermore in this section.

Sediment consolidation is another main cause of deformation, particularly in the coastal zones, which has already been demonstrated by the InSAR-derived deformation (Du et al., 2020; Ma et al., 2019). The results in this study indicate that the Guangzhou metro No.18 Line located at the tail of the Nansha district has experienced significant subsidence, which is up to 97.1 mm, as shown in section C in Fig. 8 (d). This subsidence is mainly attributed to the long-term consolidation of the alluvial clay deposits (Feng et al., 2021), and it is exacerbated by the excavation, as revealed at P05 (see Fig. 8c).

Extensive land reclamations have also been carried out in the coastal zones in Hong Kong, Macao, and Shenzhen. To investigate the ground deformation caused by land reclamation, we compare the deformation velocities derived along metro lines situated in both reclaimed and non-reclaimed lands in Shenzhen. The mean deformation velocity is calculated as almost zero for the non-reclaimed lands, while this value is –0.4 mm/year in reclaimed land, suggesting that the metro lines constructed on the reclaimed land are more susceptible to deformation than those in other regions.

(4) Other factors

Additional factors, such as grouting reinforcement and groundwater variation, may also contribute to deformation in both underlaying tunnel and ground surface.

Grouting reinforcement is a necessary geotechnical technique to avoid extensive subsidence before tunneling, or to mitigate tunneling accidences, in areas with problematic stratum, such as water-rich, soft soil, sandy cobble, silty sand, silty clay, coarse sand, and weathered granite (Dong et al., 2022). However, the ground can be uplifted when the slurry is largely inflowed and exceed pore water pressure, and this phenomenon often happens for tunnel construction in urban areas with problematic strata (Dong et al., 2022). This technique has been adopted during the metro construction in the GBA (Dong et al., 2022; He et al., 2020; Zhao et al., 2023); however, due to the lack of detailed information on grouting activities, such as injection time and slurry volume, it is difficult to capture the uplift at the obtained coherent point. We suspected that the grouting-induced uplift is happening during the period between grouting reinforcement and excavation of the foundation pit.

Groundwater variations in the aquifer system due to pumping and recharging are usually coupled with ground deformation. On the other hand, long-term tunnel deformation can cause groundwater infiltration and further damage to the tunnel, and this phenomenon is very significant in Shanghai (Shen et al., 2014). Previous studies report that the ground along metro lines in Beijing and Shanghai has suffered a long-term longitudinal deformation due to the activities associated with the local aquifer system (Duan et al., 2020; Wang et al., 2022). This deformation trend related to groundwater variation has not been observed in our results, but it cannot be excluded that the deformation is associated with fluctuation in groundwater levels at a very local scale and with differing extents, which may need further investigation.

5.2. Risk assessment

The summarized heatmap and the final risk level map are demonstrated in Fig. 13. In the final risk level map, the three risk levels account for 13.76% (L1), 2.16% (L2), and 0.39% (L3) of the buffer zone along metro lines (~1,259 km^2). The mean displacement velocities of points in the L3, L2, and L1 clusters are –6.5 mm/year, –3.4 mm/year, and –2.2 mm/year, respectively, while this value is calculated to be –0.2 mm/year for L0 cluster (83.69% of buffer zone area). These values are statistically reflecting the trend of the deformation, and the deformation velocity for a single point can deviate largely to this value.

Comparing the risk level assessment with the original displacement velocities, we can see that the high risky areas are overall confirmed to the areas with large deformation. However, there are several steps in the risk assessing method that can be optimized in the future. Firstly, the threshold applied to label the point is empirically chosen, and it leads to a larger number of points labeled as 1 (slight deformation) than that labeled as 3 (severe deformation). Moreover, the radius R is empirically set to be 1 km when creating the heatmap in this study. If this radius is set too small, there will be many zero neighboring points, which leads to an infinite value for the weight. The larger the radius, the harder for the risky levels to be differentiated.

Secondly, the risk assessment is based on point-wise data, which is selected according to their phase stability and are spatially

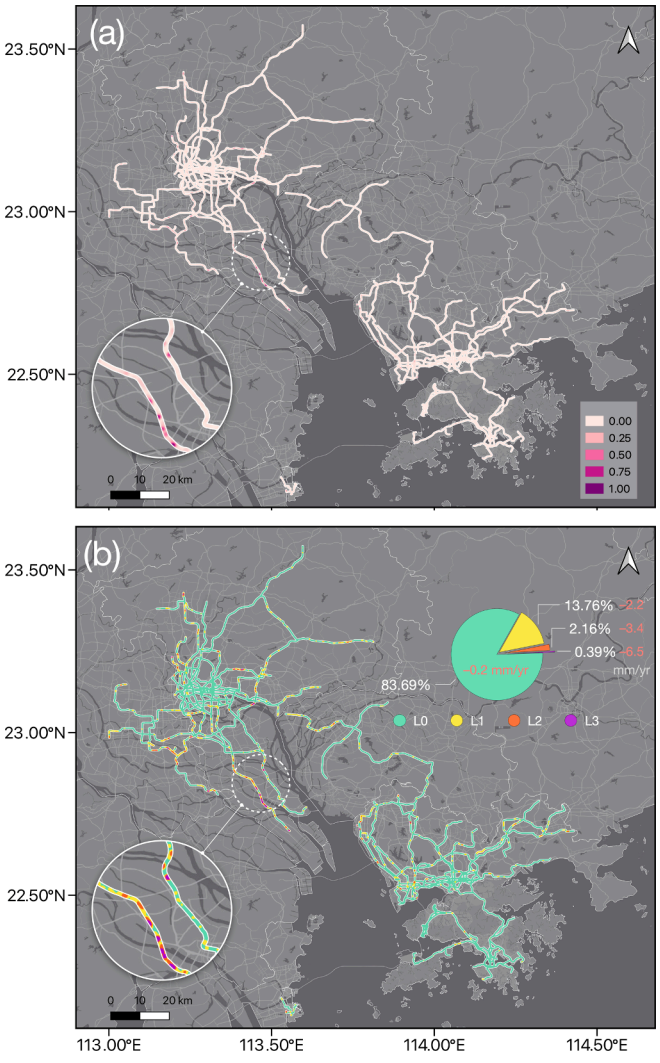

Fig. 13. (a) The weighted heatmap summarized with heatmaps for $\mathscr{L}$ = 1,2, and 3, and (b) the risk level map of metro lines within the GBA.

inhomogeneous sampled. This can be improved by using homogeneous coherent points, such as distributed scatterer InSAR (Jiang et al., 2015; Jiang and Guarnieri, 2020). Alternatively, in this study, the risky index and the total number within a small region are used as a weight in producing the heatmap to balance the point density difference. However, this can lead to underestimation of risk in areas with a large number of selected permanent scatterers, and overestimation of risk in areas with very few selected permanent scatterers.

Finally, the risk assessment is based on the InSAR-derived displacement velocity. It can reflect the severity of the land deformation along metro lines to some extent, however, InSAR-derived time-series deformation of different temporal patterns can have the same velocity, and they cannot be differentiated by using the aforementioned risk assessment. InSAR-derived deformation features strong noises and low temporal resolutions in many cases. Adaptation of time-series analysis methods should be able to deal with these difficulties in the future.

6. Conclusions

In this study, a comprehensive deformation behavior along the metro lines in the GBA, one of the most rapidly developing metropolitan areas in the world, has been presented based on the MT-InSAR derived results. Ground deformation along 42 operated and 25 under-constructed metro lines within 6 out of 11 cities in the GBA, have been revealed using multi-temporal Sentinel-1 data spanning from March 2017 to February 2022. The results indicate that the InSAR-derived LOS displacement velocities in the study areas range from –39.4 mm/year to 14.2 mm/year. The findings of this study suggest that tunnel excavation, adjacent excavation and construction, andunfavorable geological conditions are the three typical factors responsible for the deformation in the study areas. Due to lacking detailed information, deformation induced by other factors not limited to, such as grouting reinforcement and local groundwater variations, is encouraged to be explored in further study. In addition, risk assessment based on the derived InSAR deformation velocities is carried out by using the proposed MAD heatmap clustering method. The findings suggest that an area summed up to approximately 205.24 km^2 has experienced a relatively severe deformation, with 13.76%, 2.16%, and 0.39% of the area ranking as risk levels L1, L2, and L3, respectively. The mean velocities of the levels L1, L2, and L3 are –6.5 mm/year, –3.4 mm/year, and –2.2 mm/year, respectively. Future work calls for research focusing on the risk assessment of diverse deformation patterns based on deep learning methods, and detailed field information is necessary to be collected to assist research related to deformation of the metro systems.

CRediT authorship contribution statement

Bochen Zhang: Conceptualization, Methodology, Visualization, Funding acquisition, Project administration, Writing – review & editing. **Xianing Liao:** Software, Writing – original draft, Visualization, Validation. **Jiayuan Zhang:** Investigation, Validation. **Siting Xiong:** Methodology, Writing – review & editing. **Chisheng Wang:** Formal analysis. **Chuanhua Zhu:** Validation. **Jiasong Zhu:** Funding acquisition, Supervision. **Xiaoqiong Qin:** Formal analysis. **Qingquan Li:** Supervision.

Declaration of Competing Interest

The authors declare that they have no known competing financial interests or personal relationships that could have appeared to influence the work reported in this paper.

Data availability

Data will be made available on request.

Acknowledgements

This work was supported by the Guangdong Basic and Applied Basic Research Foundation (No. 2021A1515011427 and 2022A1515110861), the Shenzhen Scientific Research and Development Funding Program (Grants 20200807110745001 and 20190808120005713), the Shenzhen Metro Group Company, Limited. Scientific Research Consulting Services (STJS-DT413-KY002/2021), and the University Grants Council of the Hong Kong Polytechnic University (1-BD2S). We thank ESA/Copernicus for providing the Sentinel-1A SAR images.

References

Blewitt, G., Kreemer, C., Hammond, W.C., Gazeaux, J., 2016. MIDAS robust trend estimator for accurate GPS station velocities without step detection. J. Geophys. Res-Sol. Ea. 121, 2054–2068. https://doi.org/10.1002/2015JB012552.

Blewitt, G., Hammond, W.C., Kreemer, C., 2018. Harnessing the GPS data explosion for interdisciplinary science. Eos 99, 485. https://doi.org/10.1029/2018EO104623.

Chang, C.T., Sun, C.W., Duann, S., Hwang, R.N., 2001. Response of a Taipei Rapid Transit System (TRTS) tunnel to adjacent excavation. Tunn. Undergr. Sp. Tech. 16, 151–158. https://doi.org/10.1016/S0886-7798(01)00049-9.

Dong, Z., Zhang, X., Tong, C., Chen, X., Feng, H., Zhang, S., 2022. Grouting-induced ground heave and building damage in tunnel construction: A case study of Shenzhen metro. Undergr. Space. 7, 1175–1191. https://doi.org/10.1016/j.undsp.2022.04.002.

Du, Y., Feng, G., Liu, L., Fu, H., Peng, X., Wen, D., 2020. Understanding land subsidence along the coastal areas of Guangdong, China, by analyzing multi-track MTInSAR data. Remote Sens. 12, 299. https://doi.org/10.3390/rs12020299.

Duan, L., Gong, H., Chen, B., Zhou, C., Lei, K., Gao, M., Yu, H., Cao, Q., Cao, J., 2020. An improved multi-sensor MTI time-series fusion method to monitor the subsidence of Beijing subway network during the Past 15 Years. Remote Sens. 12, 2125. https://doi.org/10.3390/rs12132125.

Feng, W.-Q., Zheng, X.-C., Yin, J.-H., Chen, W.-B., Tan, D.-Y., 2021. Case study on long-term ground settlement of reclamation project on clay deposits in Nansha of China. Mar. Georesour. Geotec. 39, 372–387. https://doi.org/10.1080/1064119X.2019.1704319.

Ferretti, A., Fumagalli, A., Novali, F., Prati, C., Rocca, F., Rucci, A., 2011. A new algorithm for processing interferometric data-stacks: SqueeSAR. IEEE. T. Geosci. Remote 49, 3460–3470. https://doi.org/10.1109/TGRS.2011.2124465.

Gheorghe, M., Armaș, I., Dumitru, P., Călin, A., Bădescu, O., Necsoiu, M., 2020. Monitoring subway construction using Sentinel-1 data: A case study in Bucharest, Romania. Int. J. Remote Sens. 41, 2644–2663. https://doi.org/10.1080/01431161.2019.1694723.

Giardina, G., Milillo, P., DeJong, M.J., Perissin, D., Milillo, G., 2019. Evaluation of InSAR monitoring data for post-tunnelling settlement damage assessment. Struct. Control. Hlth. 26, e2285. https://doi.org/10.1002/stc.2285.

Hartigan, J.A., Wong, M.A., 1979. Algorithm AS 136: A k-means clustering algorithm. J. R. Stat. Soc. C-Appl. 28, 100–108. https://doi.org/10.2307/2346830.

He, X.-C., Xu, Y.-S., Shen, S.-L., Zhou, A.-N., 2020. Geological environment problems during metro shield tunnelling in Shenzhen. China. Arab. J. Geosci. 13, 1–18. https://doi.org/10.1007/s12517-020-5071-z.

Hooper, A., Zebker, H., Segall, P., Kampes, B., 2004. A new method for measuring deformation on volcanoes and other natural terrains using InSAR persistent scatterers. Geophys. Res. Lett. 31 (23) https://doi.org/10.1029/2004GL021737.

Hu, B., Li, Z., 2021. Time-Series InSAR Technology for Ascending and Descending Orbital Images to Monitor Surface Deformation of the Metro Network in Chengdu. IEEE J-STARS. 14, 12583–12597. https://doi.org/10.1109/JSTARS.2021.3130584.

Jiang, M., Ding, X., Hanssen, R.F., Malhotra, R., Chang, L., 2015. Fast statistically homogeneous pixel selection for covariance matrix estimation for multitemporal InSAR. IEEE T. Geosci. Remote 53, 1213–1224. https://doi.org/10.1109/TGRS.2014.2336237.

Jiang, M., Guarnieri, A.M., 2020. Distributed scatterer interferometry with the refinement of spatiotemporal coherence. IEEE T. Geosci. Remote 58, 3977–3987. https://doi.org/10.1109/TGRS.2019.2960007.

Kavvadas, M.J., 2005. Monitoring ground deformation in tunnelling: Current practice in transportation tunnels. Eng. Geol. 79, 93–113. https://doi.org/10.1016/j.enggeo.2004.10.011.

Kyriakidis, M., Hirsch, R., Majumdar, A., 2012. Metro railway safety: An analysis of accident precursors. Safety. Sci. 50, 1535–1548. https://doi.org/10.1016/j.ssci.2012.03.004.

Lancia, M., Su, H., Tian, Y., Xu, J., Andrews, C., Lerner, D.N., Zheng, C., 2020. Hydrogeology of the Pearl River Delta, southern China. J. Maps 16, 388–395. https://doi.org/10.1080/17445647.2020.1761903.

Leys, C., Ley, C., Klein, O., Bernard, P., Licata, L., 2013. Detecting outliers: Do not use standard deviation around the mean, use absolute deviation around the median. J. Exp. Soc. Psychol. 49, 764–766. https://doi.org/10.1016/j.jesp.2013.03.013.

Liang, R., Wu, W., Yu, F., Jiang, G., Liu, J., 2018. Simplified method for evaluating shield tunnel deformation due to adjacent excavation. Tunn. Undergr. Sp. Tech. 71, 94–105. https://doi.org/10.1016/j.tust.2017.08.010.

Liao, X., Zhang, B., Wu, S., 2022. Monitoring of ground deformation along Shenzhen metro system with sentinel-1A SAR imagery. In: Proc. 2022 IEEE Int. Geosci. Remote Sens. Symp. 2943-2946. https://doi.org/10.1109/IGARSS46834.2022.9884406.

Linney, L., 1983. A review of the geotechnical aspects of the construction of the first phase of the Mass Transit Railway, Hong Kong. Q. J. Eng. Geol. Hydroge. 16, 87–102. https://doi.org/10.1144/GSL.QJEG.1983.016.02.02.

Ma, P., Wang, W., Zhang, B., Wang, J., Shi, G., Huang, G., Chen, F., Jiang, L., Lin, H., 2019. Remotely sensing large-and small-scale ground subsidence: A case study of the Guangdong-Hong Kong–Macao Greater Bay Area of China. Remote Sens. Environ. 232, 111282 https://doi.org/10.1016/j.rse.2019.111282.

Marghany, M., 2012. Three-dimensional coastal geomorphology deformation modelling using differential synthetic aperture interferometry. Z. fur Naturforsch. -J. Phys. Sci. 67, 419. https://doi.org/10.5560/zna.2012-0031.

Marghany, M., 2014. Simulation of three-dimensional of coastal erosion using differential interferometric synthetic aperture radar. Glob. NEST J. 16, 80–86. https://doi.org/10.30955/gnj.001055.

Marghany, M., 2014a. Hybrid Genetic Algorithm of Interferometric Synthetic Aperture Radar For Three-Dimensional Coastal Deformation, SoMeT, pp. 116-131. https://doi.org/10.3233/978-1-61499-434-3-116.

Miller, J., 1991. Reaction time analysis with outlier exclusion: Bias varies with sample size. Q. J. Exp. Psychol.: Hum. Exp. Psych. 43, 907–912. https://doi.org/10.1080/14640749108400962.

Perissin, D., Wang, Z., Lin, H., 2012. Shanghai subway tunnels and highways monitoring through Cosmo-SkyMed Persistent Scatterers. ISPRS J. Photogramm. 73, 58–67. https://doi.org/10.1016/j.isprsjprs.2012.07.002.

Ren, D.-J., Shen, S.-L., Cheng, W.-C., Zhang, N., Wang, Z.-F., 2016. Geological formation and geo-hazards during subway construction in Guangzhou. Environ. Earth. Sci. 75, 1–14. https://doi.org/10.1007/s12665-016-5710-6.

Shen, S.-L., Wu, H.-N., Cui, Y.-J., Yin, Z.-Y., 2014. Long-term settlement behaviour of metro tunnels in the soft deposits of Shanghai. Tunn. Undergr. Sp. Tech. 40, 309–323. https://doi.org/10.1016/j.tust.2013.10.013.

Sousa, R.L., Einstein, H.H., 2021. Lessons from accidents during tunnel construction. Tunn. Undergr. Sp. Tech. 113, 103916 https://doi.org/10.1016/j.tust.2021.103916.

Wang, H., Feng, G., Xu, B., Yu, Y., Li, Z., Du, Y., Zhu, J., 2017. Deriving spatio-temporal development of ground subsidence due to subway construction and operation in delta regions with PS-InSAR data: A case study in Guangzhou. China. Remote Sens. 9, 1004. https://doi.org/10.3390/rs9101004.

Wang, Y., Jiao, J.J., 2012. Origin of groundwater salinity and hydrogeochemical processes in the confined Quaternary aquifer of the Pearl River Delta. China. J. Hydrol. 438, 112–124. https://doi.org/10.1016/j.jhydrol.2012.03.008.

Wang, R., Yang, M., Dong, J., Liao, M., 2022. Investigating deformation along metro lines in coastal cities considering different structures with InSAR and SBM analyses. Int. J. Appl. Earth. Obs. 115, 103099 https://doi.org/10.1016/j.jag.2022.103099.

Werner, C., Wegmüller, U., Strozzi, T., Wiesmann, A., 2000. Gamma SAR and interferometric processing software, Proc. ERS-Envisat Symp., Gothenburg, Sweden. Citeseer, p. 1620. Available online: https://www.gamma-rs.ch/uploads/media/2000-1_GAMMA_Software.pdf.

Wu, S., Yang, Z., Ding, X., Zhang, B., Zhang, L., Lu, Z., 2020. Two decades of settlement of Hong Kong International Airport measured with multi-temporal InSAR. Remote Sens. Environ. 248, 111976 https://doi.org/10.1016/j.rse.2020.111976.

Wu, S., Zhang, B., Liang, H., Wang, C., Ding, X., Zhang, L., 2021. Detecting the Deformation Anomalies Induced by Underground Construction Using Multiplatform MT-InSAR: A Case Study in To Kwa Wan Station. Hong Kong. IEEE J-STARS. 14, 9803–9814. https://doi.org/10.1109/JSTARS.2021.3113672.

Yang, M., Wang, R., Li, M., Liao, M., 2022. A PSI targets characterization approach to interpreting surface displacement signals: A case study of the Shanghai metro tunnels. Remote Sens. Environ. 280, 113150 https://doi.org/10.1016/j.rse.2022.113150.

Zhao, Y., Chen, X., Hu, B., Huang, L., Li, W., Fan, J., 2023. Evolution of tunnel uplift and deformation induced by an upper and collinear excavation: A case study from Shenzhen metro. Transp. Geotech. 39, 100953 https://doi.org/10.1016/j.trgeo.2023.100953.

Zhou, Z., Irizarry, J., 2016. Integrated framework of modified accident energy release model and network theory to explore the full complexity of the Hangzhou subway construction collapse. J. Manage. Eng. 32, 05016013. https://doi.org/10.1061/(ASCE)ME.1943-5479.0000431.

Zhou, Z., Irizarry, J., Zhou, J., 2021. Development of a database exclusively for subway construction accidents and corresponding analyses. Tunn. Undergr. Sp. Tech. 111, 103852 https://doi.org/10.1016/j.tust.2021.103852.

Zhou, J., Xiao, H., Jiang, W., Bai, W., Liu, G., 2020. Automatic subway tunnel displacement monitoring using robotic total station. Measurement 151, 107251. https://doi.org/10.1016/j.measurement.2019.107251.

Zhu, W., Zhang, Y., Liu, Z., Zhu, Q., 2020. Pre-and postcollapse ground deformation revealed by sar interferometry: a case study of foshan (China) ground collapse. J. Sensors 2020, 1–17. https://doi.org/10.1155/2020/8899054.

Zhu, Y., Zhou, J., Zhang, B., Wang, H., Huang, M., 2022. Statistical analysis of major tunnel construction accidents in China from 2010 to 2020. Tunn. Undergr. Sp. Tech. 124, 104460 https://doi.org/10.1016/j.tust.2022.104460.